AGU PUBLICATIONS

JGR

Journal of Geophysical Research: Oceans

RESEARCH ARTICLE

10.1002/2015JC011501

Observations of seasonal subduction at the Iceland-Faroe Front

N. L. Beaird[1], P. B. Rhines[2], and C.C. Eriksen[2]

[1]Department of Physical Oceanography, Woods Hole Oceanographic Institution, Woods Hole, Massachusetts, USA, [2]School of Oceanography, University of Washington, Seattle, Washington, USA

Key Points:
- Glider observations of previously unknown seasonal subduction at Iceland Faroe Front
- Low salinity water mass subducts in winter when mixed layers are deep
- Heat and salt fluxes comparable to previous eddy estimates

Correspondence to:
N. Beaird,
nbeaird@whoi.edu

Citation:
Beaird, N. L., P. B. Rhines, and C. C. Eriksen (2016), Observations of seasonal subduction at the Iceland-Faroe Front, *J. Geophys. Res. Oceans*, *121*, 4026–4040, doi:10.1002/2015JC011501.

Received 24 NOV 2015
Accepted 4 MAY 2016
Accepted article online 6 MAY 2016
Published online 12 JUN 2016

Abstract The polar front in the North Atlantic is bound to the ridge between Iceland and the Faroe Islands, where about one-half of the northward transport of warm Atlantic Water into the Nordic Seas occurs, as well as about one sixth of the equatorward dense overflow. We find a low salinity water mass at the surface of the Iceland-Faroe Front (IFF), which in wintertime subducts along outcropping isopycnals and is found in much modified form on the Atlantic side of the Iceland-Faroe Ridge (IFR) crest. The features found on the Atlantic side of the crest at depth have temperature and salinity characteristics which are clearly traceable to the surface outcrop of the IFF. The presence of coherent low salinity layers on the Atlantic side of the IFR crest has not been previously reported. Warm waters above the IFR primarily feed the Faroe Current, and injection of a low salinity water mass may play an early role in the water mass transformation taking place in the Nordic Seas. The seasonality of the intrusive features suggests a link between winter convection, mixed layer instability and deep frontal subduction. These low salinity anomalies (as well as a low oxygen water mass from the Iceland Basin) can be used as tracers of the intermediate circulation over the IFR.

1. Introduction

In the northern North Atlantic, light and dense waters of the Atlantic Meridional Overturning Circulation are in many places separated by upper ocean fronts, most of which are strongly influenced by the presence of steep topography. Frontal processes in these regions impact meridional heat and salt transport and water mass modification, and therefore map onto larger scale ocean circulation and climate. In this paper we report observations of seasonal stirring of water masses across an important frontal boundary between the North Atlantic and the Nordic Seas.

The Greenland-Scotland Ridge separates the North Atlantic from the Nordic Seas and Arctic mediterranean, and its potential vorticity signature influences the frontal structure and circulation between the basins. The North Atlantic is predominantly warm and saline, whereas north of the Greenland-Scotland Ridge intense atmospheric forcing produces large volumes of cold and relatively fresh waters. Subtropical Atlantic waters arrive at the ridge through the complex pathways of the subpolar/subtropical gyre boundary [*Brambilla and Talley*, 2008]. Meridional flow across the Greenland-Scotland Ridge and subsequent water mass transformation comprise the northern downwelling branch of the Atlantic Meridional Overturning Circulation, where poleward flowing surface waters of Atlantic origin are transformed by interaction with the atmosphere, returning equatorward as newly formed dense water [*Mauritzen*, 1996].

The widest gap (∼300 km) in the Greenland-Scotland Ridge is the Iceland-Faroe Ridge (IFR), the hydrography of which is dominated by the Iceland-Faroe Front (IFF, Figure 1). The IFF marks the boundary between the North Atlantic waters and Nordic waters at depths shallower than the IFR crest (∼450 m) [*Read and Pollard*, 1992]. Roughly locked to the IFR crest, the isopycnals of the IFF slope up and northeastward from the ridge (Figure 2). The presence of dense overflow water on the Atlantic side of the IFR means that some frontal isopycnals continue Atlantic-ward of the ridge crest, lying nearly parallel to the IFR topography [*Beaird et al.*, 2013]. The warm Atlantic Water adopts an anticyclonic meandering pathway feeding the Faroe Current which is a response to the steep topography, both from vortex squashing as it encounters the ridge, and in feeding the cyclonic boundary current system of the Nordic Seas. The estimate of the mean surface geostrophic circulation in Figure 1 has been constructed from satellite altimetry, surface drifters and hydrography from AVISO maps of absolute dynamic topography. The altimeter products were produced by

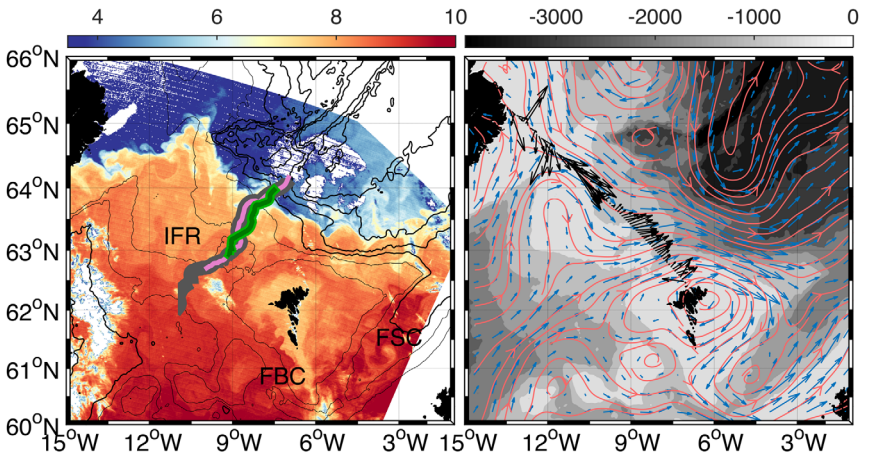

Figure 1. A MODIS sea surface temperature (°C) image of the Iceland-Faroe Ridge region on (left) 14 May 2009 and (right) 1992–2010 mean geostrophic surface velocity (blue vectors and pink streamlines) from AVISO mean dynamic topography. Black vectors are the mean ADCP upper 150 m averaged velocity from Childers et al. 2014. (right) Bathymetry is shaded in gray colorscale. Geographic features are labeled. Bathymetric contours are shown every 500 m. The gray, green and pink lines in the left plot indicate the glider path taken in Figures 2–4 (gray), and 12 (pink, green).

Ssalto/Duacs and distributed by Aviso, with support from Cnes (http://www.aviso.altimetry.fr/duacs/). It suggests two dominant pathways for poleward flow of Atlantic Water across the IFR: in the northwest close to Iceland; and a broader, possibly stronger stream in the southeast close to the Faroe Islands. Anticyclonic

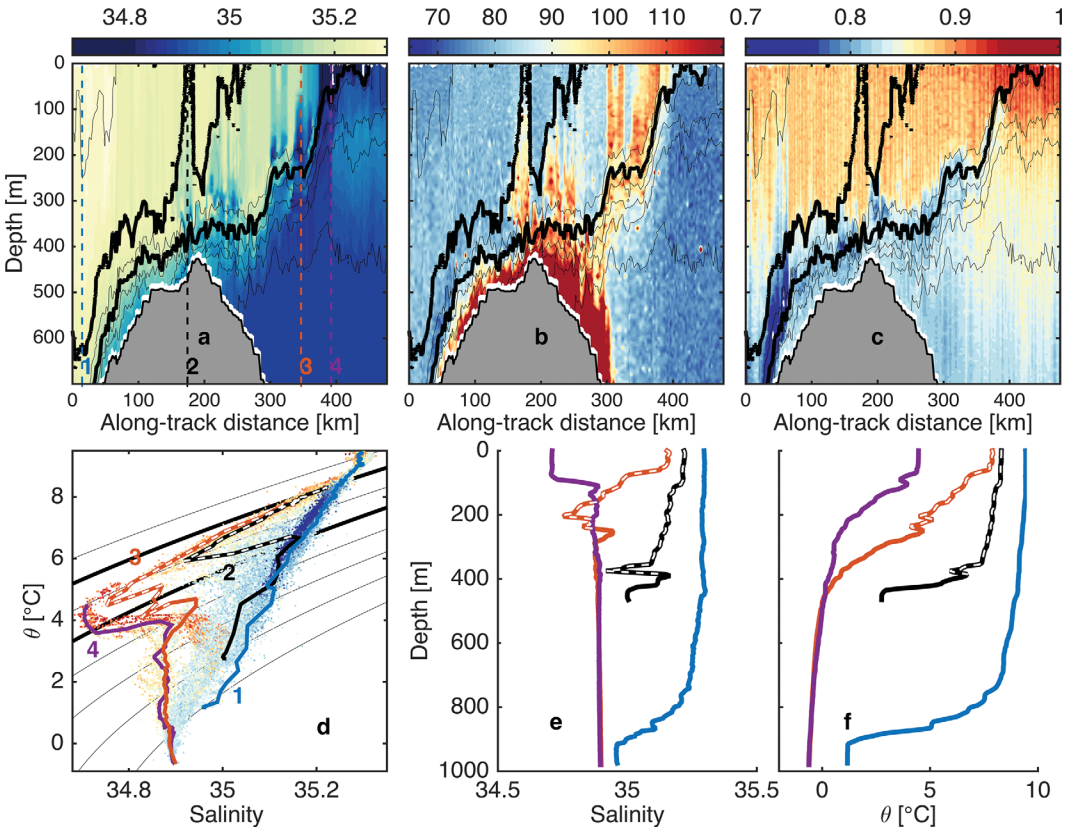

Figure 2. The Iceland-Faroe Ridge and Iceland-Faroe Front in a wintertime glider section (2–19 December 2007, along gray line in Figure 1) perpendicular to the ridge, with the Iceland Basin on the left and Nordic Seas on the right. (a) Salinity, (b) red backscatter (counts) and (c) Oxygen saturation (as a fraction) along the section with isopycnals contoured in 0.1 kg m^{-3} increments from 1027.3 to 1028 kg m^{-3}, with 1027.4 and 1027.6 kg m^{-3} in bold. (d) Potential Temperature-Salinity relation for the section, with color showing oxygen saturation (same scale as Figure 2c). Example profiles of potential temperature versus salinity, salinity versus depth and potential temperature versus depth in Figures 2d, (e and f) correspond to the profiles labeled in Figure 2a. The intrusive layers in example profiles 2 and 3 are indicated with white dashes.

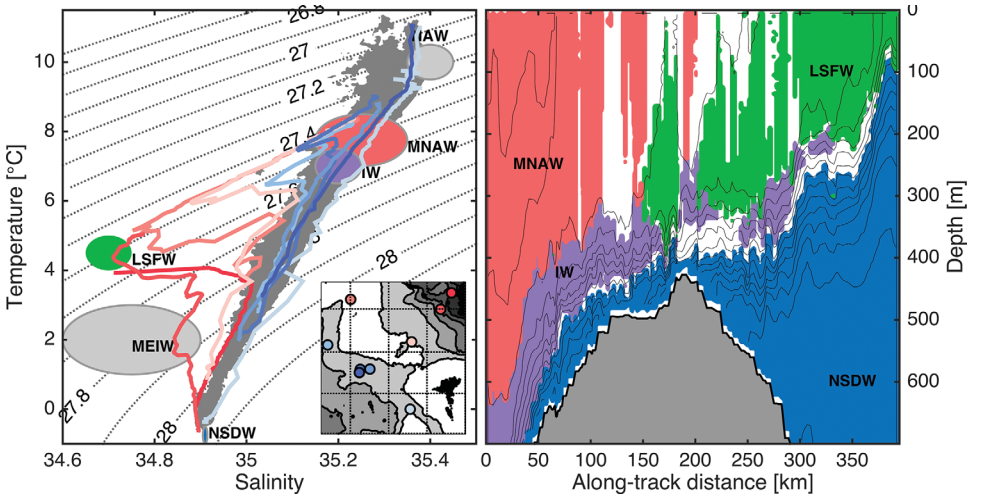

Figure 3. (left) Example θ-S profiles from around the IFR showing the variable influence of low salinity intermediate waters from north of the IFR crest. Locations of the profiles are shown in matching colored dots in inset map. Typical ranges of some water mass properties are shown in light gray ellipses. 95% of all θ-S points from the Atlantic side of the IFR fall within the dark gray contour shown in the background. (right) schematic distribution of the water masses discussed in the text, labeled and approximately delineated on the section in Figure 2 (along gray line in Figure 1). White regions where water masses are mixed to a degree to not be properly represented by a single label. Black contours show selected isopycnals. Water masses include Modified North Atlantic Water (pink, MNAW), Iceland Basin Intermediate Water (purple, IW), the Low Salinity Frontal Water and associated thermohaline intrusions discussed in this paper (green, LSFW), and Norwegian Sea Deep Water and overflow water (blue, NSDW). We show the overflow on the Atlantic side of the IFR in blue even though it contains NSDW as well as other waters.

retroflection at the northwest end of the ridge deflects the flow temporarily equatorward. Velocity sections from the ferry Norröna (black vectors overlaid on Figure 1) by *Rossby and Flagg* [2012] show striking agreement, and are consistent with the presence of a near-Iceland branch. The unequivocal presence of warm surface waters near Iceland (Figure 1) however shows that Atlantic Water does reach across the IFR by both pathways.

The front slopes more steeply in the west, where it sometimes coincides with the Jan Mayen front [*Hansen and Østerhus*, 2000], and gradually becomes more diffuse toward the Faroe side of the IFR [*Read and Pollard*, 1992]. Geostrophic balance at the IFF supports the Faroe Current, carrying about 3.8 Sv (half) of the inflow of Atlantic water to the Nordic Seas [*Hansen et al*., 2003; *Rossby and Flagg*, 2012; *Hansen et al*., 2015]. The surface expression of the front, typically defined as the surface salinity $S = 35$ isohaline, exhibits significant variability in position on weekly to monthly timescales, but does not appear to vary seasonally [*Smart*, 1984; *Hansen and Meincke*, 1979].

The IFF is baroclinically unstable [*Allen et al*., 1994; *Allen and Smeed*, 1996], producing large meanders and a vigorous eddy field [*Hansen and Meincke*, 1979; *Rossby et al*., 2009] (apparent in the sea surface temperature of Figure 1). Poleward flow of Atlantic waters exhibits a slight preference for crossing at the northwestern ridge where the IFR abuts the Icelandic plateau [*Perkins et al*., 1998] and at the relatively deep part of the IFR near the Faroe Plateau [*Rossby et al*., 2009]. Cold, fresh, polar waters are carried to the western end of the front by the East Iceland Current [*Jónsson*, 2007].

On the Atlantic side of the Iceland Faroe Ridge, the typical water mass structure in potential temperature-salinity (θ-S) space is a quasi-linear mixing line (Figure 3, see dark gray patch) between the relatively light Atlantic waters and the dense Nordic Seas overflow layer above the seabed. The observations reported here reveal a more complicated seasonally variable water mass configuration, disrupting the typical two layer structure. Low salinity waters from north of the ridge appear as mid depth thermohaline intrusions in winter, skewing the quasi-linear θ-S curve toward a low salinity end member in the potential density anomaly range $27.4 \leq \sigma_\theta \leq 27.65$ kg m^{-3}. While fresh waters at the IFF have been described before, we believe these data to be the first evidence tracing the water mass across the IFR crest, and the first evidence of seasonality to the exchange.

Low salinity waters of polar origin have been described in the IFF region by numerous authors [*Meincke*, 1978; *Read and Pollard*, 1992; *Hallock*, 1985; *Allen and Smeed*, 1996]. The freshest waters in the IFF region

arrive there from the direction of Iceland, and are either composed of runoff/meltwater from Iceland itself, or, more likely, modified polar waters of the East Greenland Current carried to the front by the East Icelandic Current [*Jónsson*, 2007; *Macrander et al*., 2014]. Relatively fresh water enters the IFF in the west and subducts along isopycnals as it is advected along the front in the surface layer [*Meincke*, 1978; *Read and Pollard*, 1992]. Of particular relevance here are the studies by *Hallock* [1985], who discusses intrusive interleaving of low salinity water at the front and the associated cross front fluxes, and *Meincke* [1978] who traces the subducting low salinity water at the IFF. Similar low salinity intrusive features are a prominent feature of the data set discussed in this paper.

The paper begins with a description of the observations used, and a discussion of the character and seasonality of the observed thermohaline intrusions. Possible mechanisms producing the intrusions are then discussed, as well as rough estimates of the heat and salt fluxes associated with the subduction and their relative importance with respect to previous observations at the front. Finally, conclusions are drawn.

2. Measurements

Between November 2006 and November 2009, quarterly deployments (February, June, September, November) of Seaglider autonomous underwater vehicles were made in the region of the Iceland-Faroe Ridge. The resulting data set consists of over 17,000 full-depth hydrographic profiles (more details can be found in *Beaird et al*. [2013]). Of these, about 10,000 were located on the Iceland-Faroe Ridge and will be considered here. The remainder were made north of the Faroe Islands and in the Faroe-Shetland Channel. The Seaglider is an autonomous 1000 m depth rated profiling glider capable of long duration missions [*Eriksen et al*., 2001]. The glider makes sawtooth profiles with a horizontal to vertical aspect ratio of about three to one. During these deployments gliders took samples every 20 s ($\sim$1.5 m vertical resolution) of temperature, conductivity, pressure, dissolved oxygen, red and blue wavelengths of optical backscatter and fluorescence. Geostrophic shear and relative geostrophic velocity can be calculated from adjacent density profiles. The expected surfacing location of a glider after a dive/climb cycle can be calculated from a flight model tuned for the glider [*Eriksen et al*., 2001]. By taking the vector difference between the expected surfacing position after a dive/climb cycle and the actual surfacing position determined by GPS location, the glider returns an estimate of the depth-averaged velocity encountered during its dive. The depth average of the relative geostrophic velocity is referenced to the depth average velocity estimate from the flight model and GPS to produce absolute geostrophic velocities. Deployments were primarily made in the FBC region after which the gliders were directed along the Atlantic side of the IFR toward Iceland. Occasionally cross-ridge sections were occupied. The gliders remained on the ridge shallower than the 1000 m isobath and did not sample farther out in the Iceland Basin.

3. Observations

3.1. Water Mass Structure on the Atlantic Side of the Front

On the Atlantic side of the Iceland-Faroe Ridge crest warm, salty, Atlantic waters are situated above cold, dense water overflow of Nordic Seas/Arctic origin (Figures 2 and 3). In the mean, Atlantic waters flow northward into the Nordic Seas, and the polar waters flow equatorward into the Iceland Basin. Locally, however, the circulation is largely along topographic contours (into and out of the page in Figure 2), and thus not necessarily immediately North/South, but the final result of the circulation is meridional exchange.

The Atlantic waters include Modified North Atlantic Water (MNAW) and the Intermediate Water (IW) of the Iceland Basin [*Hansen and Østerhus*, 2000; *van Aken and de Boer*, 1995] (Table 1 and Figure 3). The majority of the Atlantic layer is made up of MNAW, a relatively weakly stratified subpolar mode water formed in wintertime in the subpolar gyre from subtropical waters transported by the Gulf Stream/North Atlantic Current [*Read and Pollard*, 1992; *Brambilla et al*., 2008]. Intermediate Water resides in the permanent pycnocline of the Iceland Basin and is 'biogeochemically defined': having no characteristic temperature or salinity distinction from MNAW, IW is apparent as an oxygen minimum in the range T=6−8°C, S=35.1−35.25, and σ_θ= 27.55−27.65 kg m^{-3}, as in Figure 2c [*van Aken and de Boer*, 1995; *Sarafanov et al*., 2008]. The oxygen minimum is a widespread feature throughout the subtropical North Atlantic sourced from upwelling zones off the African coast, and marks water coming north in the North Atlantic Current from deep in the subtropics [*Johnson and Gruber*, 2007; *Stendardo and Gruber*, 2012]. In the Iceland Basin proper, IW marks the extent of

Table 1. Regional Water Mass Property Ranges[a]

Acronym	Name	Temperature Range	Salinity Range	Notes
NSDW	Norwegian Sea Deep Water	−1.03°C	34.91	
LSFW	Low Salinity Frontal Water	∼4.5°C	∼34.7	High O_2 & backscatter
MEIW	Modified East Icelandic Water	1 → 3°C	34.6 → 34.9	
NI/AI	N. Icelandic Winter/Arctic Intermediate water	≥ 3°C	≤ 34.78	
EICW	East Icelandic Current Water	8°C	34.3	
MNAW	Modified North Atlantic Water	7 → 8.5°C	35.1 → 35.3	subpolar mode water
NAW	North Atlantic Water	9.5 → 10.5°C	35.35 → 35.45	
IW	Iceland Basin Intermediate Water	6 → 8°C	35.1 → 35.25	Low O_2
ISOW	Iceland-Scotland Overflow Water	2.7 → 2.9°C	34.92	

[a]*Fogelqvist et al*. [2003]; *Hansen and Østerhus* [2000]; *Read and Pollard* [1992].

the deepest wintertime mixing, and contrasts sharply with the ventilated winter mixed layers. We identify IW by its low oxygen signature, which, being a minimum, cannot be produced by mixing of other water types in the region. IW, though found deeper in the Iceland Basin, has been shown to ascend onto the IFR by *Ullgren et al*. [2014].

3.2. Fresh Thermohaline Intrusions

The low salinity thermohaline intrusions found seasonally on the Atlantic side of the IFF can be distinguished by their anomalous temperature, salinity, backscatter, and oxygen characteristics. The intrusions are fresh, cool, and oxygen rich relative to the North Atlantic waters in the potential density anomaly range $27.4 \leq \sigma_\theta \leq 27.65$ kg m^{-3}, which include both MNAW and IW (Figure 2). The intrusions also have relatively high backscatter in red wavelengths (Figure 2b). This middepth maximum in backscatter associated with the intrusions is unrelated to the higher backscatter in the bottom boundary layer above the IFR associated with suspended sediment carried by bottom intensified currents. Potential temperature-salinity (θ-S) curves from profiles which contain intrusions show fresh anomalies relative to the quasi-linear curves connecting Atlantic and overflow waters (Figures 2d and 3). The intrusions skew the θ-S curve in the potential density anomaly range $27.4 \leq \sigma_\theta \leq 27.65$ kg m^{-3} toward a point with a temperature and salinity of about $\approx$ 4.5°C and $\approx$ 34.7. We will refer to this unmodified source of the low salinity features as Low Salinity Frontal Water (LSFW), and refer to modified LSFW 'intrusions' on the Atlantic side of the IFF surface outcrop since the LSFW features intrude between (and mix with) layers of Atlantic water. The least modified LSFW is found at the surface along the IFF (Figure 2a, upper 100 m, in the last 25 km and Figures 2d–2f, example profile 4) and at the northwestern end of the IFR near the Iceland shelf.

Away from the front, the intrusions are readily apparent as wedge-like shapes in the θ-S curve, laying within the triangle defined by the θ-S points (8.2, 35.2), (4.5, 34.7), and (3.75, 35) (Figure 3). The Atlantic 'background' θ-S relation is typically tight and almost linear between 27.4 and 27.65, making low salinity anomalies conspicuous even when their magnitude is quite small. The 'top' of the wedge in θ-S space is formed by mixing of LSFW with overlying MNAW, producing the gradual reduction of the salinity anomaly with increasing temperature. The 'bottom' of the wedge is formed by the boundary between fresh anomaly and the low oxygen, high salinity, IW situated below the intrusion.

The strength of the thermohaline intrusion is indicated by the difference in salinity along an isopycnal (isopycnal salinity anomaly, $S'_\sigma = S(\sigma) - S_{ATL}(\sigma)$) from a quasi-linear Atlantic reference θ-S relation defined from profiles which are manually determined not to contain intrusions ($S_{ATL}(\sigma)$). Figure 4 shows that the cross-frontal section of S'_σ decreases in strength with distance from the IFF surface outcrop. The total anomalous freshwater content contained in the intrusions can be calculated by integrating the isopycnal salinity anomaly relative to the Atlantic reference salinity over the depth range of the intrusions:

$$\mathrm{FWC}'_\sigma = \int_{z27.65}^{z27.4} \frac{S(\sigma) - S_{ATL}(\sigma)}{S_{ATL}(\sigma)} dz \quad (1)$$

where the limits of integration are the depths of the two isopycnals that bound the intrusions. Figure 4 shows the anomalous freshwater contained in the intrusions for the cross-ridge section.

The provenance of the low salinity surface water is unclear. *Hansen and Østerhus* [2000] in their review discuss multiple relatively cold, fresh water masses that converge at the IFF from the direction of Iceland and

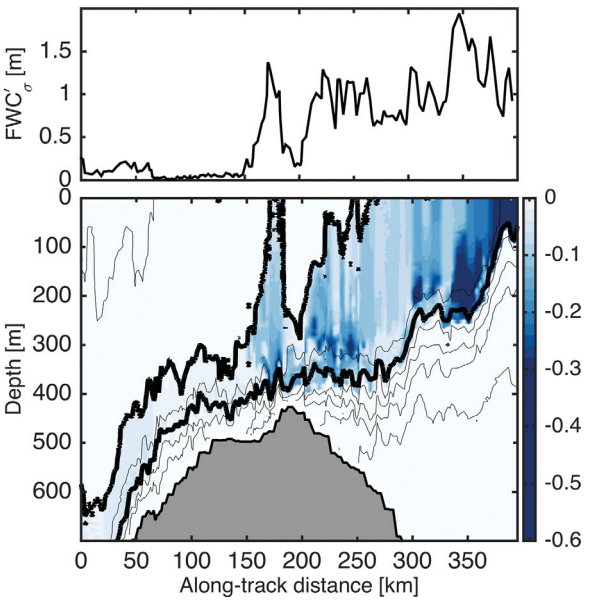

Figure 4. (top) Integrated freshwater content anomaly (equation (1)) in the isopycnal range 27.4–27.65 kg m^{-3} along the cross-IFR section shown in Figure 2 (along gray line in Figure 1). (bottom) Isopycnal salinity anomaly (S'_σ) in the same density range. Isopycnals are contoured in 0.1 kg m^{-3} increments from 1027.3 to 1028 kg m^{-3}, with 1027.4 and 1027.6 kg m^{-3} in bold.

whose admixture is most commonly called Modified East Icelandic Water (MEIW Table 1) [*Read and Pollard*, 1992]. MEIW is typically dense enough to be considered part of the overflow from the Nordic Seas into the North Atlantic (the overflow is usually defined by potential density, $\sigma_\theta \geq 27.8$ kg m^{-3}). Significant variability in the composition of the water mass leads to a generally broad definition of its properties.

We consider the low salinity water masses observed by the gliders to be a part of the MEIW in the sense that it is a modified (by mixing) form of a variety of low salinity waters which are advected east along the IFF from the direction of Iceland. However the intrusions discussed here are not as dense as the 'canonical' MEIW. Slightly warmer and fresher than the North Icelandic Winter water/Arctic Intermediate water (NI/AI) described by *Meincke* [1978], the low salinity water mass of interest is likely some mixture of NI/AI and East Icelandic Current water (EIC) [*Read and Pollard*, 1992] and thus might fit into a relatively warm, fresh category of MEIW. *Allen et al.* [1994] describe patches of cold fresh water ($S = 34.4$ and $T = 4$°C) at the northwest end of the IFF in the upper 50 m of the water column. They suggest the water mass comes from Icelandic fresh water runoff and ice melt carried to the front by the East Icelandic Current. It seems likely that this is a constituent of the low salinity water described here. *Read and Pollard* [1992] also note that in the summer, freshwater at the front spreads over the top of the Atlantic water to the south. Investigation of the relatively rare sea surface temperature images collected on clear days often reveals filaments of cold water streaming off the Icelandic shelf into the IFF [cf. *Perkins et al.*, 1998;, *Scott and McDowall*, 1990]. All the constituent water masses are known to have significant interannual variability [*Hansen and Østerhus*, 2000], and perhaps a 'typical' definition of MEIW is impractical. Purely for convenience in this paper we describe the source of the thermohaline intrusions discussed below as LSFW, but argue that this is just one of the constituents of MEIW, and not a 'new' water mass in any sense.

The least modified LSFW is found at the surface outcrop of the IFF, but the features are found at greater depth on the Atlantic side of the IFR. Therefore some vertical as well as horizontal circulation influences the intrusions. The anomaly section in Figure 4 crosses the IFR and IFF (Figure 1, gray line), and shows several stages in the evolution of LSFW into the thermohaline intrusions found toward the Atlantic side of the IFR. The initial subduction and formation of the thermohaline intrusions north of the IFR can be seen at $\geq$ 300 km into the section. A low salinity tongue extends down from the LSFW at the surface, along the 27.45 isopycnal. LSFW intrudes below the MNAW and mixes with it, creating the typical wedge-like thermohaline intrusion (Figure 3), with the greatest salinity anomaly near the bottom of the feature. The example profiles 4 and 3 in Figure 2 show the transition from surface LSFW (profile 4, with surface low salinity) to thermohaline intrusion (profile 3 with the salinity minimum below the MNAW). Figure 2c shows the close proximity of the oxygen rich LSFW features and the oxygen depleted IW. IW is seen in varying intensities rising along the 27.5 isopycnal toward the IFF. Several more highly modified thermohaline intrusions are seen further to the southwest in Figure 4, on both sides of the ridge crest (between 200 and 300 m depth at ~200 km along the section).

From the stages of development of the intrusions in Figure 4 a few characteristics of the thermohaline intrusions emerge: the intrusions subduct from the surface layer of the IFF to depths of 300 m (and eventually 600–800 m on the Atlantic side of the IFR); they are modified by mixing with MNAW close to the front; and

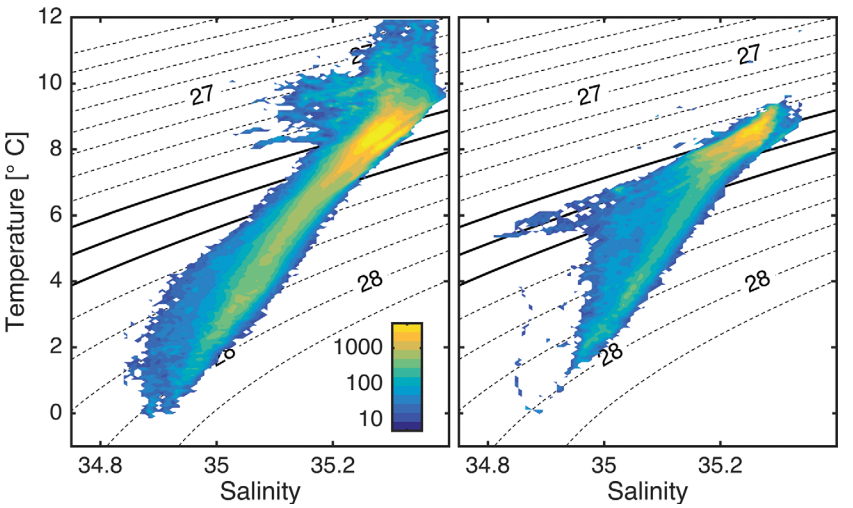

Figure 5. Potential Temperature-Salinity histograms for profiles determined to contain (right) a LSFW thermohaline intrusion and (left) those without an intrusion. Contours are the number of points in 0.006 PSU by 0.0065°C bins. Potential density is contoured in the background in 0.1 kg m^{-3} increments, with the isopycnal range of 27.4–27.65 kg m^{-3} in bold.

they become significantly thicker (∼300 m) than the LSFW layer at the IFF (∼100 m). It should be noted that advection of the features in this section should not be mistaken as two dimensional. As mentioned above, the mean circulation in the region is along topographic contours (perpendicular to this cross ridge section), and a complicated three dimensional eddying circulation will be responsible for the advection of the features discussed in Figure 4 (see, the complex nature of the SST front in Figure 1).

3.2.1. Statistics of Thermohaline Intrusions

Example sections on the Atlantic side of the IFR (Figure 2) show parcels of LSFW are still clearly identifiable, though mixing with MNAW has eroded the minimum S'_σ considerably (from ~ -0.55 to ~ -0.1). Due to significant variability in the strength of the salinity anomaly, combined with noisy salinity data (due to thermal inertia effects in the un-pumped glider conductivity cell), an objective identification routine for LSFW thermohaline intrusions proved elusive. However, the distinctive shape of the intrusion θ-S relation, with the trajectory of the θ-S curve toward LSFW and the intensification of the salinity anomaly at the bottom of the intrusion, makes LSFW influence readily identifiable by eye. All glider profiles on the Atlantic side of the IFR during the 3 year field campaign were manually sorted into a group that contained LSFW thermohaline intrusions and a group that did not. Over the ridge 1972 profiles were found to have LSFW influence, compared with 8131 without. Figure 5 demonstrates the difference in θ-S space between profiles with and without LSFW intrusions, showing histograms of IFR θ-S profiles with (right) and without (left) LSFW intrusions. Several differences between the θ-S groups are apparent right away. The most obvious is the skewness toward a point at T ≈ 4.5°C and S ≈ 34.7 – the definition of LSFW. This is obviously the signal by which the groups were classified. Also, the seasonal thermocline is present in the intrusion free group and absent in the intrusion group. This is the first hint that the LSFW thermohaline intrusions occur in winter.

It is important to note that no source of low salinity water in this density range exists on the Atlantic side of the IFR. This is further evidence, along with the similarity in θ-S characteristics to LSFW and the observed stages of subduction in Figure 2, that the thermohaline intrusions observed southwest of the front represent advection from the Nordic Seas side of the ridge. *Ullgren et al*. [2014] discuss a low salinity intermediate water which interacts with the FBC overflow. This water mass appears to be a mixture of IW and the Labrador Sea Water that sits below the permanent pycnocline in the Iceland Basin. The low salinity water described in that paper (State III type profiles, cf. *Ullgren et al*. [2014, Figure 12]) is denser than and distinct from what we report here.

3.3. Seasonality and Geographic Distribution of Intrusions

Figure 6 depicts both the seasonal (right) and geographic (left) distribution of the identified LSFW intrusions (the groups in Figure 12 5). Profiles containing LSFW thermohaline intrusions are indicated in red, the intrusion free group in blue. Two significant patterns in the distribution of thermohaline intrusions are evident.

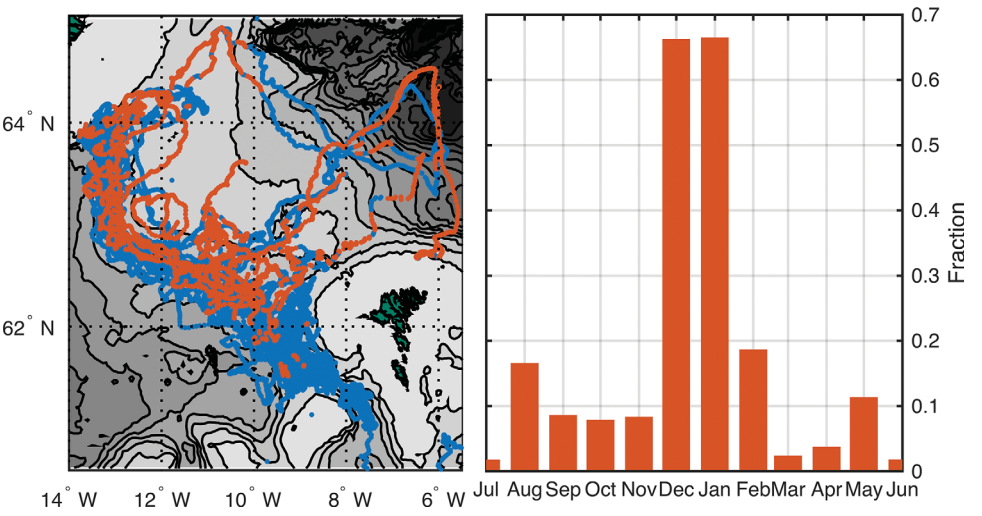

Figure 6. (left) geographic distribution of profiles with identified LSFW thermohaline intrusions in the potential density anomaly range $27.4 \leq \sigma_\theta \leq 27.65$. Each dot represents a glider profile where red points show profiles with intrusions, blue profiles without. (right) Seasonal distribution of the fraction of profiles with intrusions.

The first is that profiles with LSFW influence are almost completely restricted to the IFR north and west of 62°N, 10°W – outside the Faroe Bank Channel outflow region. This pattern implies advection of LSFW thermohaline intrusions across the IFR rather than through the Faroe-Shetland and Faroe Bank Channels. Low salinity waters from the IFF do arrive in the Iceland Basin via the Faroe Shetland Channel to Faroe Bank Channel pathway but these waters are heavily modified by mixing [*Meincke*, 1978; *Borenäs et al*., 2001; *Ullgren et al*., 2014] and lose the sharp intrusive character of the features identified on the Atlantic side of the IFR crest in Figure 5 (right). The Faroe Shetland Channel to Faroe Bank Channel pathway is independent of the one reported in this paper. Figure 6 provides evidence that the LSFW intrusive features cross the IFR crest rather than transit through the Faroese Channels.

The second new observation is that nearly all the identified intrusions are found between November and February (Figure 6, right). The seasonality perhaps obscures these features from the observational record on the IFR, with its bias toward summer months. In December and January low salinity intrusions are found in ∼65% of profiles made on the Atlantic side of the IFR. When the FBC outflow region is excluded from the census (LSFW intrusions are not found there, even in winter), 80% of profiles on the Atlantic side of the IFR contain some evidence of LSFW influence in December and January, and 40% in November and February. Thermohaline intrusions are almost completely absent between March and October. The seasonal pattern repeats itself in each of the 3 years of the study. Figure 7 shows the total number of profiles on the Atlantic side of the IFR in 30 day segments and the number of profiles with LSFW intrusions. There is a spike in observations of intrusions centered on each of the three Januarys, and very few occurrences the rest of the year.

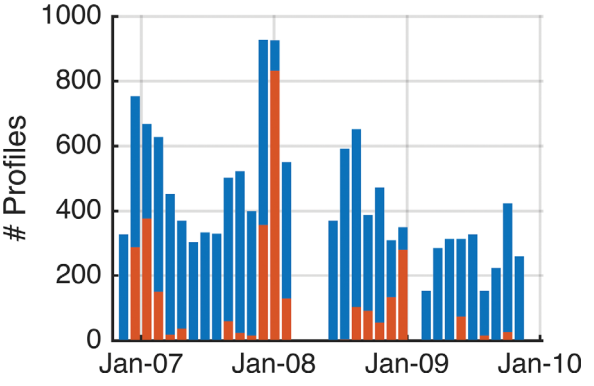

Figure 7. The total number of profiles on the Atlantic side of the IFR in 30 day bins (blue) and the number of profiles with identified thermohaline intrusions (red). The full period of the field study is shown.

Seasonal histograms of all θ-S profiles from the Atlantic side of the IFR outside the FBC outflow region are shown in Figure 8. Again the intrusions are apparent primarily in early winter. Similar θ-S histograms for the FBC outflow region alone (Figure 9) show that no low salinity intrusive features are found in that region. The FBC θ-S curves suggest that there are no significant seasonal changes in either the FBC overflow or the upper layer Atlantic water (aside from the growth and decay of the seasonal thermocline). This

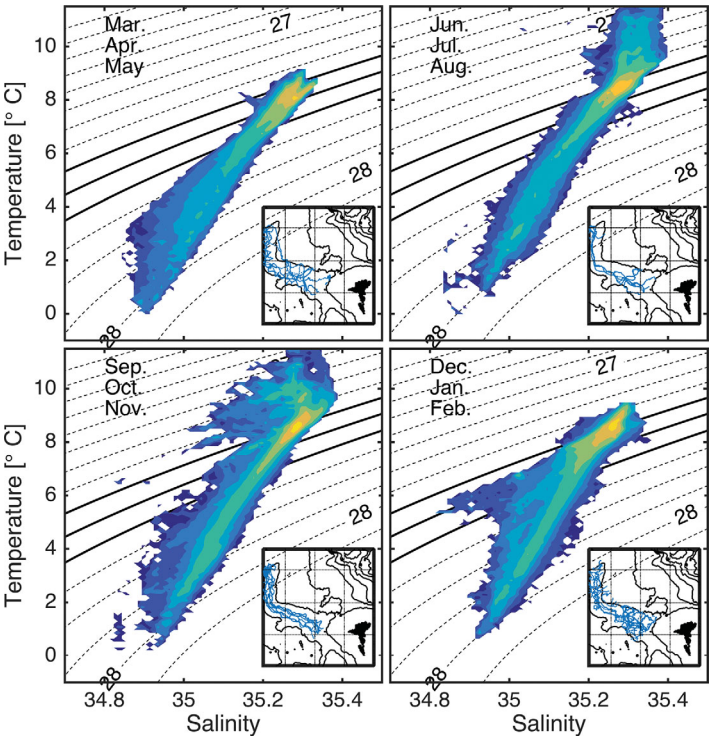

Figure 8. Histogram of all θ-S profiles from the Atlantic side of the IFR, excluding the FBC outflow region. Profiles are broken into 3 month seasons. The locations of profiles are shown as blue dots in the inset maps.

further supports the conjecture of seasonal injection of LSFW across the IFR, making it unlikely that the features arrive via the FBC or are the result of seasonal changes in the Atlantic waters, changes which would also be apparent in the upper layer of the FBC.

The seasonal cycle of mixed layer depth and mean freshwater content anomaly on the Atlantic side of the IFR is displayed in Figure 10. Only profiles made outside the FBC outflow region are included. The freshwater content anomaly (FWC'_σ) is calculated as in equation (1), but the S_{ATL} is calculated independently for each glider from the set of profiles that do not contain intrusions. Mixed layer depths are calculated following *de Boyer Montégut* [2004]. A strong seasonal cycle of mixed layer depth and FWC'_σ is apparent. Wintertime mixing is intense in the region southwest of the IFF surface outcrop, with mixed layers reaching $\geq$600 m [see also *Brambilla et al.*, 2008]. Figure 10 shows that the appearance of LSFW intrusions on the Atlantic side of the IFR (higher FWC'_σ) in late November coincides with the deepening of the mixed layer.

Some variation exists in the geographic distribution of the strength of the thermohaline intrusions. Figure 11 shows the integrated freshwater content anomaly (equation (1)) for each glider profile in the data set, broken into the groups with and without intrusions. For the profiles containing intrusions the largest anomalous freshwater content tends to be near the surface outcrop of the IFF, northeast of the ridge, and also near the Iceland shelf at the northern edge of the ridge.

The extent to which the LSFW intrusions reach farther to the south and west in the Iceland basin cannot be determined from this data set. The gliders only occupied the region of the IFR shallower than the 1000 m isobath, and by chance the late fall and early winter profiles, when LSFW was observed, tended to be slightly shallower, above the 900 m isobath. This sampling bias does not allow observation of LSFW intrusions at the south and westernmost extent of the data (Figure 6).

4. Discussion

The preceding observations suggest the existence of substantial stirring in the upper water column of water masses originating on the cold and warm sides of the IFF. They also demonstrate a clear seasonality to the advection of low salinity water that is subducted away from the IFF surface outcropping position. The distribution and layering of these water masses of Nordic and Atlantic origin demonstrate the vertical complexity of the frontal region of the IFR.

The LSFW intrusions are carried toward the Atlantic side of the IFR crest, but the ultimate fate of the intrusions is likely not permanent residence in the Iceland Basin. Much of the upper water column above the IFR, into which the LSFW intrudes, eventually joins the Faroe Current and is advected into the Nordic Seas [*Rossby et al.*, 2009; *Rossby and Flagg*, 2012]. So, although the glider observations do indicate that the

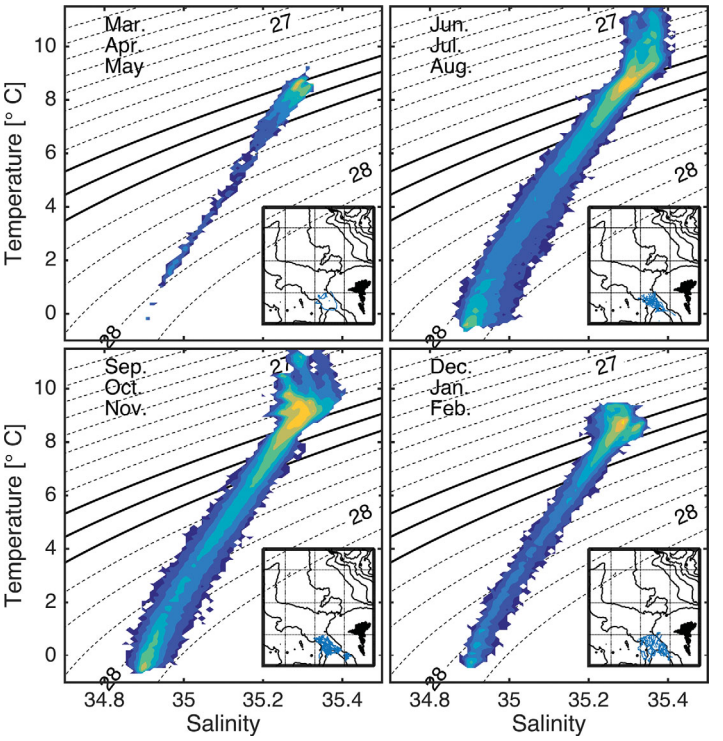

Figure 9. Histogram of all θ-S profiles from the FBC outflow region. Profiles are broken into 3 month seasons. The locations of profiles are shown as blue dots in the inset maps.

intrusive features are found on the Atlantic side of the IFR crest, they become embedded in the poleward flow into the Norwegian Sea.

In this section, possible mechanisms forcing the frontal subduction will be discussed, and a rough order of magnitude calculation will be made showing that the flux of LSFW is a locally important cross frontal mechanism for heat and salt exchange.

4.1. Possible Mechanisms of Subduction

Subduction of LSFW intrusions at the front implies ageostrophic vertical velocities at the IFF. Vertical motions at the front have been shown to occur by *Allen and Smeed* [1996], who used high resolution SeaSoar surveys and the omega equation to diagnose vertical velocity in the meanders and eddies of the IFF. That study revealed large vertical velocities up to 100 m d^{-1} in the isopycnal range σ_θ=27.4−27.65, the level of the LSFW intrusions. This frontal ageostrophic circulation is in all likelihood partially responsible for the subduction of LSFW seen by the gliders.

Lack of full-field synoptic velocity data during the glider surveys prevents unequivocal determination of the intrusive dynamics. Cross-track absolute geostrophic velocity is available from the glider, but the expectation is that ageostrophic circulation plays an important role in transporting and subducting the LSFW intrusions. In order to solve the omega equation, synoptic along and across-front density information is needed, but only four isolated cross-front sections were made. However, we can describe plausible mechanisms responsible for the observed circulation and seasonality based on previous studies of cross frontal exchanges.

The path of the Atlantic waters crossing the IFR (Figure 1) is curved, making the front three-dimensional, strongly reacting to the ridge topography. Nevertheless, several familiar instabilities are likely at work: baroclinic instability on the poleward side of the ridge, as well as Mixed Layer Instabilities (MLIs) arising from deep wintertime convection and horizontal stratification [*Boccaletti et al*., 2007]. *Hansen and Meincke* [1979]; *Allen et al*. [1994]; *Willebrand and Meincke* [1980], and *Rossby et al*. [2009] all provide arguments for classic baroclinic instability of the IFF, where regions of opposing potential vorticity gradient overlie one another.

The importance of submesoscale, unbalanced motion in transferring properties both horizontally and vertically has received substantial attention. This type of motion, involving large vertical velocities and small scale filamentous structure, is active in flows with large Rossby numbers ($O(1)$). Meanders and eddies in the IFR region have the requisite large relative vorticity ($\sim$0.8 f) [*Allen and Smeed*, 1996] and Rossby numbers, and SST images reveal ubiquitous cross frontal filamentation [*Scott and McDowall*, 1990; *Niiler*, 1992].

Subduction at upper ocean fronts is driven both through external atmospheric forcing (buoyancy or wind stress) and through internal frontal instability. Externally, a down front windstress will produce Ekman transport which drives dense water over light, causing turbulent mixing and ageostrophic circulation [*Thomas and Lee*, 2005]. Internally, mesoscale eddy induced shear and strain disturb geostrophic balance and

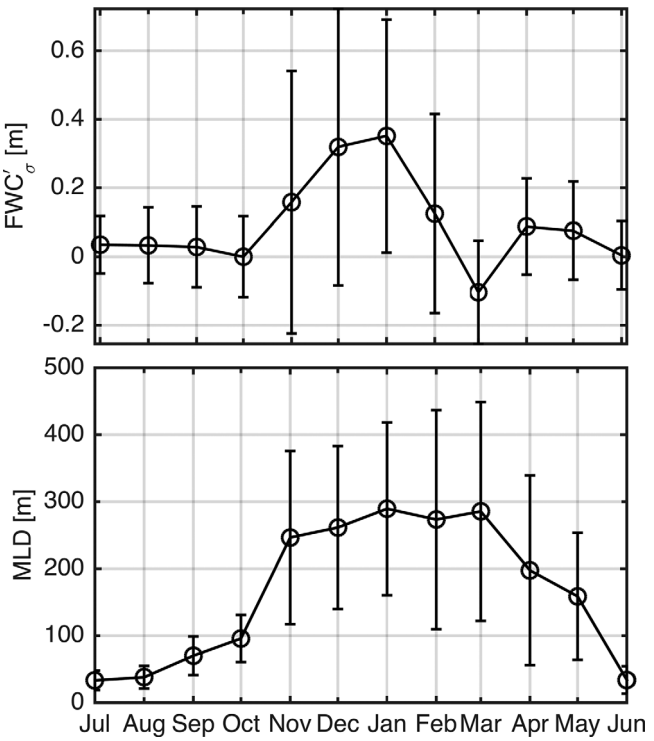

Figure 10. Monthly averaged properties on the Atlantic side of the IFR (excluding the FBC region): (top) mean freshwater content anomaly integrated over the potential density anomaly range $27.4 \leq \sigma_\theta \leq 27.65$; (bottom) mixed layer depth calculated using the method of *de Boyer Montégut* [2004]. Bars show one standard deviation.

generate ageostrophic vertical motions to restore that balance [*Hoskins et al.*, 1978; *Pollard and Regier*, 1992]. Confluent flow in unstable and meandering fronts leads to local frontogenesis and ageostrophic vertical circulation [*Hoskins et al.*, 1978]. This ageostrophic circulation due to internal instability has been shown to cause subduction of waters from the cold side of the front under waters of the warm side [*Spall*, 1995]. Detailed observations of the process at work at the northern flank of the Gulf Stream by *Thomas and Joyce* [2010] show the production of "cusp-like" thermohaline intrusions with characteristics remarkably similar to those observed here.

A second set of instabilities is relevant to subduction at the IFF. It is possible that Mixed Layer Instabilities [*Boccaletti et al.*, 2007] play a role in this winter time cross-frontal exchange. MLIs are a class of instability which occur in regions with lateral inhomogeneities coincident with vertically well mixed layers. A region with horizontal density gradients (e.g., a front) that becomes vertically well mixed by strong atmospheric forcing will undergo adjustment where the vertical isopycnals slump due to gravity. The slumping is arrested by the establishment of geostrophic balance. *Boccaletti et al.* [2007] show that the adjusted state is susceptible to submesoscale baroclinic instability. One of the primary differences between MLI and traditional baroclinic instability is in scale: MLIs only impact the upper (well mixed) portion of the water column, while the baroclinic instability of the IFF, say, will extend throughout

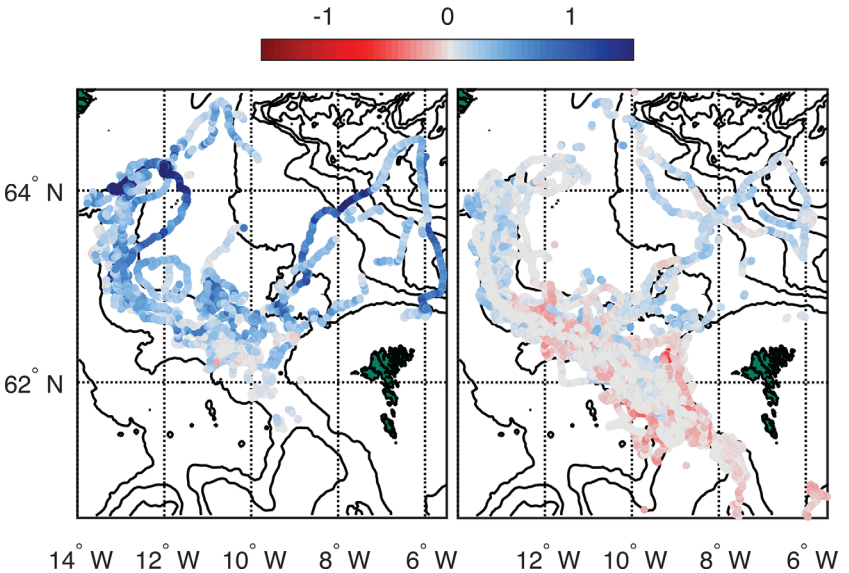

Figure 11. Freshwater content anomaly [m] in the isopycnal range 27.4–27.65 kg m^{-3} (equation (1)) for each glider dive. (left) The group of profiles that contain intrusions, and (right) the group which does not contain intrusions.

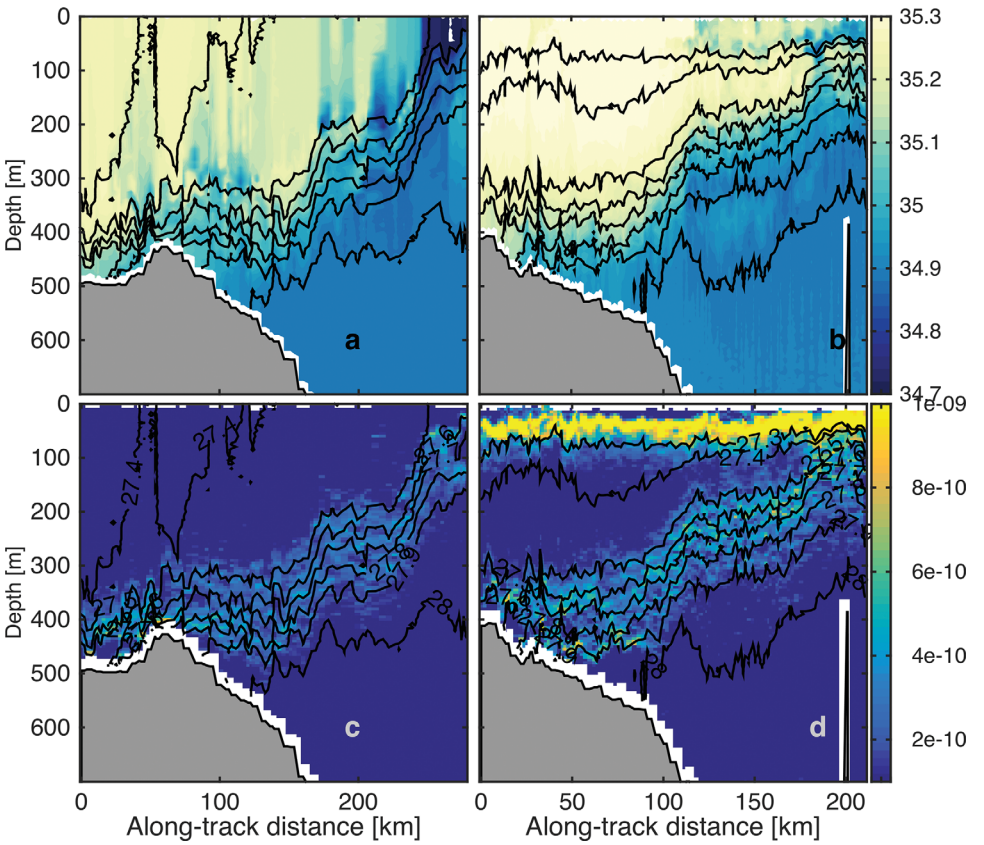

Figure 12. (a, b) Salinity and (c, d) planetary potential vorticity ((m s)$^{-1}$) at the IFF in winter (left column, along pink line in Figure 1) and summer (right column, along green line in Figure 1) sections.

the depth of the front. However at the IFF, wintertime mixed layers can reach depths comparable to the front, and thus the MLI scales approach those of instabilities of the IFF itself. MLIs also have faster timescales than baroclinic instability. At the IFF in winter the conditions for MLI are met, with strong horizontal density gradients and deep wind driven mixed layers (Figure 12). In the IFF case, the MLI would be occurring on top of the steeply sloping front, as opposed to the gentle sloped thermocline case described in *Boccaletti et al.* [2007].

An idealized numerical model of the Iceland-Faroe Front and IFR suggests that MLIs could provide the seasonality of the observed LSFW subduction. The model shows that in winter the scales of the mixed layer eddies become comparable to the scales of the baroclinic instability in the front, and that MLIs dominate over instability of the front [*Jimenez-Urias and Thompson*, 2016]. The mixed layer eddies are seen to drive a residual ageostrophic overturning circulation in the density ranges of the LSFW intrusions. The MLI overturning streamfunction in the model extends farther toward the Atlantic side of the IFR crest than the overturning associated with instabilities of the main IFF density front, and thus is consistent with both the seasonality and extent of the intrusion observations reported here.

It seems very likely that the seasonal nature of the LSFW subduction is related to the deepening of the surface mixed layer. Observational and modeling studies show a seasonal cycle in submesoscale energy with wintertime enhancement that can influence vertical exchange with the ocean interior [*Callies et al.*, 2015]. Southwest of the frontal outcrop the mixed layer reaches down to the densities of the IW in the Iceland basin, up to 600 m in places (Figure 10). Northeast of the IFF the mixed layer is much shallower, but is still 75 m deep. In the winter, the strong potential vorticity barrier of the seasonal thermocline is erased (Figure 12). There is a strong potential vorticity gradient on the isopycnals in question (σ_θ=27.4−27.65) in the summer, but in winter the potential vorticity on the intermediate isopycnals is low even as the front is crossed. There is still a salinity gradient on the isopycnals, but in winter the surface expression of the IFF is associated with vertical isopycnals and a transition between the very deep mixed layers to the southwest, and the relatively shallow mixed layer to the northeast.

4.2. Basic Heat and Salt Flux Estimates

A back-of-the-envelope estimate of the heat and salt flux due to the subducting LSFW can be made by using vertical velocity data from *Allen and Smeed* [1996]. As mentioned above, meandering at fronts forces vertical velocities which can subduct properties slantwise along isopycnals [*Pollard and Regier*, 1990, 1992; *Spall*, 1995; *Thomas and Joyce*, 2010; *Thomas et al*., 2010]. *Allen and Smeed* [1996] calculated ageostrophic vertical velocities of 25–100 m d^{-1} at the IFF using the three dimensional omega equation. We take these velocities as the vertical component of a slantwise along-isopycnal flow, and assume the mean isopycnal slope of the IFF to be 0.01 (it is steeper in the west, and shallower in the east [*Read and Pollard*, 1992]), giving ageostrophic cross-front velocities that are roughly in the range 0.03–0.12 m s^{-1}. We assume these ageostrophic velocities are responsible for the initial subduction and cross-frontal flux of LSFW. Close inspection of the front suggests the thickness of the initial subducting LSFW of about 40 m. We find the resulting intrusions all along the Atlantic side of the IFR (Figure 6), so we make the assumption that intrusive features occur everywhere along the ~300 km of the IFF. Heat and salt flux estimates can then be made by multiplying the width, thickness, speed, heat or salt anomaly together and dividing by the area of the IFR gap (~300 km wide, by ~500 m deep). The unmodified LSFW isopycnal salinity anomaly is ~−0.55 psu and the isopycnal temperature anomaly ~−3.5°C (e.g., Figure 3). Approximating 1 psu ≈ 1‰=1 g per kg of water, and using a reference density ρ_o=1027.45 kgm^{-3} and the specific heat of seawater C_p=3850 J/(kg°C), rough estimates of the heat and salt flux due to subducting LSFW in winter can be made. The resulting winter time cross-IFF salt flux due to LSFW is in the range 1.35–5.4 g $m^{-2}s^{-1}$ (positive values refer to northward fluxes, or here: to southward flow of cold and fresh anomalies). The associated heat flux is 3.3×10^4 to 13.3×10^4 W m^{-2}. These values can be compared with previous estimates of cross IFF fluxes. The LSFW fluxes are seasonal, and should be adjusted to annual averages to compare with other flux estimates. Using Figure 6 as a proxy for the fraction of the year when LSFW is being subducted at the front suggests the process is active 20% of the time. Therefore the annual average values for salt and heat flux, respectively, become 0.3–1.1 g $m^{-2}s^{-1}$ and 0.65×10^4 to 2.65×10^4 W m^{-2}.

The estimates of heat and salt fluxes due to subduction of LSFW are rough, and made with a number of assumptions, the most tenuous of which perhaps is the use of *Allen and Smeed* [1996] omega equation results to obtain ageostrophic cross-IFF velocities. However, numerous observations of strong ageostrophic circulation at unstable ocean fronts suggests that large vertical velocities are present. *Thomas et al*. [2010] find that vertical velocities inferred from the quasigeostrophic omega equation underestimate the vertical circulation at fronts, which suggests the estimates produced here may be low. Unknown errors in the flux magnitude arise due to assumptions about the horizontal velocity of the intrusions. However, we at least know the sign of the estimates is robust: the heat and salt flux estimates are based on temperature and salinity anomalies that are well measured; and the sign of the velocities toward the Atlantic can be inferred from the distribution of LSFW relative to its source at the IFF outcropping region.

The importance of the seasonal LSFW flux can be assessed by comparing the rough estimates above with previously published estimates of flux by mesoscale and submesoscale motions at the IFF. Three studies present such estimates: *Willebrand and Meincke* [1980], *Hallock* [1985], and *Allen et al*. [1994]. *Willebrand and Meincke* [1980] find a northward eddy heat flux of 12×10^4 W m^{-2} from a near bottom current meter moored just north of the IFR crest. Those authors claim the eddy heat flux is of the same order of magnitude as the mean equatorward advection of NSDW across the ridge, and as the heat loss from the Norwegian Sea due to the advection of low salinity water investigated by *Meincke* [1978] (although no such calculation is explicitly presented in *Meincke* [1978]). *Hallock* [1985] calculates heat and salt transport across the front by mixing in intrusive interleaving features at the IFF. *Hallock* [1985] uses the method of *Joyce* [1977], which balances vertical diffusion across intrusions (using an assumed vertical diffusivity) with horizontal cross front advection, to find salt and heat fluxes of 1.58 g $m^{-2}s^{-1}$ and 5.16×10^4 W m^{-2} respectivly. The final estimate of eddy heat and salt flux comes from *Allen et al*. [1994]. They calculate the mean salt and heat content of eddies near the IFF and estimate an eddy generation rate to get fluxes. The resulting flux estimates are 3.5 g $m^{-2}s^{-1}$ and 8.0×10^4 W m^{-2} for salt and heat.

All these flux estimates are of the same order of magnitude. Our range of estimates are also of the same order. The seasonal values are right within the range of the three previous heat flux estimates and the two salinity estimates. The annual mean fluxes reported here are smaller (particularly the heat flux) than the range in the literature. The low end of our annual estimates are roughly 10% of the values from the

literature, and 50–100% on the high end. Still, it appears that subduction and cross frontal exchange of LSFW is a significant local contribution to cross frontal flux in winter time. *Willebrand and Meincke* [1980] note that these eddy fluxes are locally important to the IFF region, but at least in the case of heat, are a small contribution to the overall budget of the Norwegian Sea. *Rossby and Flagg* [2012] estimate the total heat and salt inflow to the Nordic Seas to be 171 TW and 1.45×10^8 kg s^{-1}. *Hansen et al.* [2003] estimate higher values of 247 TW and 2.43×10^8 kg s^{-1} and *Østerhus et al.* [2005] find 313 TW and 3.03×10^8 kg s^{-1}. Assuming a width of 300 km and depth of 500 m for the IFR, the total heat and salt transport due to the subducting LSFW is 0.97–3.97 TW and $0.45–1.8\times10^5$ kg s^{-1}. The mesoscale and submesoscale fluxes at the front appear not to be comparable to the large scale advection of Atlantic waters into the Nordic Seas, but may play a role in setting local conditions. For example, *Hansen et al.* [2003] note a decrease in long-term average salinity (0.02–0.04) and temperature (0.25–0.5°C) of the MNAW core measured at the Faroe Bank (south of the IFR) and at 6°W, north of the Faroes. This cooling and freshening could be due in part to mixing of MNAW and LSFW thermohaline intrusions, as well as air-sea exchange. The rough calculation of intrusive heat fluxes above, in the annual mean, could cool the 3.8 Sv of Atlantic water inflow by 0.06–0.19°C, and freshen it by 0.01–0.03 psu.

5. Conclusions

Seaglider surveys reveal a seasonal subduction of low salinity features from the surface outcropping of the Iceland-Faroe Front across the Iceland Faroe Ridge crest that occurs only in wintertime. The anomalously fresh water subducts from the surface mixed layer forming thermohaline intrusions in the layer of Modified North Atlantic Water on the warm side of the front. The intrusions become tall and bottom intensified, recognizable in θ-S space as low isopycnal temperatures and salinities. The features are only found between November and February above the IFR outside the FBC outflow region. The subduction initiates after the onset of deep winter mixing of the surface layer. In December and January, 80% of profiles contain thermohaline intrusions, 40% of profiles in November and February do. Almost no intrusions are detected outside those 4 months. The thermohaline intrusions are found in each of the three winters during the glider field campaign (2006–2009). The intrusive features mix into the Modified North Atlantic Waters and are likely carried back into the Nordic Seas via the Faroe Current, but are on the opposite side of the front from where they originate. Some of the densest portion of the intrusions may mix into the overflow waters and travel into the deep North Atlantic.

We speculate that subduction of the low salinity water at the front is driven by ageostrophic motion associated with instabilities of the IFF, as well as mixed layer instabilities at the surface front. The destruction of the strong potential vorticity barrier of the seasonal thermocline by winter time mixing likely results in the seasonality of the signal. Rough calculations of the annual average heat and salt fluxes produced by the features are 0.65×10^4 to 2.65×10^4 W m^{-2} and -0.3 to 1.1 g m^{-2}s^{-1}. These values are slightly smaller than previous flux estimates due to mesoscale and submesoscale variability at the IFF [*Willebrand and Meincke*, 1980; *Hallock*, 1985; *Allen et al.*, 1994]. Seasonally, the fluxes are the same size as the previous estimates. This suggests that at least locally, the seasonal subduction of the low salinity surface water mass is an important contribution to cross frontal exchange.

Acknowledgments
The authors would like to thank the two anonymous reviews who have helped improve the paper. We also thank Kirk O'Donnell, Bill Fredericks, and James Bennett for help with data collection and processing. We thank Miguel Jimenez-Urias for discussion of his numerical modeling results. Additional thanks are owed to the crew of the *R.V. Magnus Heinason*, and Bogi Hansen, and Hjálmar Hátún for considerable help from the Faroe Islands. This work has been generously supported by National Science Foundation, OCE Division, through grants OCE-1029344 and OCE-0550584. The Seaglider data used in this study are freely available from the National Oceanographic Data Center (www.nodc.noaa.gov).

References

Allen, J. T., and D. A. Smeed (1996), Potential vorticity and vertical velocity at the Iceland-Faroes Front, *J. Phys. Oceanogr.*, *26*, 2611–2634.
Allen, J. T., D. A. Smeed, and A. L. Chadwick (1994), Eddies and mixing at the Iceland-Faroes Front, *Deep Sea Res., Part I*, *41*, 51–79.
Beaird, N. L., P. B. Rhines, and C. C. Eriksen (2013), Overflow waters at the Iceland–Faroe Ridge observed in multiyear seaglider surveys, *J. Phys. Oceanogr.*, *43*(11), 2334–2351, doi:10.1175/JPO-D-13-029.1.
Boccaletti, G., R. Ferrari, and B. Fox-Kemper (2007), Mixed layer instabilities and restratification, *J. Phys. Oceanogr.*, *37*(9), 2228–2250, doi:10.1175/JPO3101.1.
Borenäs, K. M., I. L. Lake, and P. A. Lundberg (2001), On the intermediate water masses of the Faroe–Bank Channel Overflow, *J. Phys. Oceanogr.*, *31*(7), 1904–1914.
Brambilla, E., and L. D. Talley (2008), Subpolar mode water in the northeastern Atlantic: 1. Averaged properties and mean circulation, *J. Geophys. Res.*, *113*, C04025, doi:10.1029/2006JC004062.
Brambilla, E., L. D. Talley, and P. E. Robbins (2008), Subpolar mode water in the northeastern Atlantic: 2. Origin and transformation, *J Geophys. Res.*, *113*, C04026, doi:10.1029/2006JC004063.
Callies, J., R. Ferrari, J. Klymak, and J. Gula (2015), Seasonality in submesoscale turbulence, *Nat. Commun.*, *6*, 6862, doi:10.1038/ncomms7862.

Childers, K. H., C. N., Flagg, and T. Rossby (2014), Direct velocity observations of volume flux between Iceland and the Shetland Islands, *J. Geophys. Res.: Oceans*, *119*(9), 5934–5944.
de Boyer Montégut, C. (2004), Mixed layer depth over the global ocean: An examination of profile data and a profile-based climatology, *J. Geophys. Res.*, *109*, C12003, doi:10.1029/2004JC002378.
Eriksen, C. C., T. J. Osse, R. D. Light, T. Wen, T. W. Lehman, P. L. Sabin, J. W. Ballard, and A. M. Chiodi (2001), Seaglider: A long-range autonomous underwater vehicle for oceanographic research, *IEEE J. Oceanic Eng.*, *26*, 424–436.
Fogelqvist, E., J. Blindheim, T. Tanhua, S. Østerhus, E. Buch, and F. Rey (2003), Greenland-Scotland overflow studied by hydro-chemical multivariate analysis, *Deep Sea Res., Part I*, *50*, 73–102.
Hallock, Z. R. (1985), Variability of frontal structure in the southern Norwegian Sea, *J. Phys. Oceanogr.*, *15*, 1245–1253.
Hansen, B., and J. Meincke (1979), Eddies and meanders in the Iceland-Faroe Ridge area, *Deep Sea Res., Part A*, *26*, 1067–1082.
Hansen, B., and S. Østerhus (2000), North Atlantic-Nordic Seas exchanges, *Prog. Oceanogr.*, *45*(2), 111–208.
Hansen, B., S. Østerhus, H. Hátún, R. Kristiansen, and K. M. H. Larsen (2003), The Iceland-Faroe inflow of Atlantic water to the Nordic Seas, *Prog. Oceanogr.*, *59*, 443–474.
Hansen, B., K. M. H. Larsen, H. Hátún, R. Kristiansen, E. Mortensen, and S. Østerhus (2015), Transport of volume, heat, and salt towards the Arctic in the Faroe Current 1993–2013, *Ocean Sci.*, *11*, 743–757, doi:10.5194/os-11-743-2015.
Hoskins, B. J., I. Draghici, and H. C. Davies (1978), A new look at the ω-equation, *Q. J. R. Meteorol. Soc.*, *104*, 31–38.
Jimenez-Urias, M., and L. Thompson (2016), An idealized study of the seasonality of frontal instabilities with implications for the Polar Front over the Iceland Faroe Ridge, paper PO24B-2952 presented at the 2016 Ocean Sciences Meeting, 2016 Ocean Sciences Meeting, AGU/ASLO/TOS, New Orleans, La., 21–27 Feb.
Johnson, G. C., and N. Gruber (2007), Decadal water mass variations along 20°W in the Northeastern Atlantic Ocean, *Prog. Oceanogr.*, *73*(3-4), 277–295, doi:10.1016/j.pocean.2006.03.022.
Jónsson, S. (2007), Volume flux and fresh water transport associated with the East Icelandic Current, *Prog. Oceanogr.*, *73*(3-4), 231–241, doi:10.1016/j.pocean.2006.11.003.
Joyce, T. M. (1977), On the lateral mixing of water masses, *J. Phys. Oceanogr.*, *7*, 626–629.
Macrander, A., H. Valdimarsson, and S. Jónsson (2014), Improved transport estimate of the East Icelandic Current 2002-2012, *J. Geophys. Res. Oceans*, *119*, 3407–3424, doi:10.1002/2013JC009517.
Mauritzen, C. (1996), Production of dense overflow waters feeding the North Atlantic across the Greenland-Scotland Ridge. Part 1: Evidence for a revised circulation scheme, *Deep Sea Res., Part I*, *43*, 769–806.
Meincke, J. (1978), On the distribution of low salinity intermediate waters around the Faroes, *Dtsch. Hydrogr. Z.*, *31*, 50–64.
Niiler, P. P. (1992), Sea surface temperature variability of the Iceland-Faeroe Front, *J. Geophys. Res.*, *97*(C11), 17,777–17,785.
Østerhus, S., W. R. Turrell, S. Jónsson, and B. Hansen (2005), Measured volume, heat, and salt fluxes from the Atlantic to the Arctic Mediterranean, *Geophys. Res. Lett.*, *32*, L07603, doi:10.1029/2004GL022188.
Perkins, H., T. S. Hopkins, S. A. Malmberg, P. M. Poulain, and A. Warn-Varnas (1998), Oceanographic conditions east of Iceland, *J. Geophys. Res.*, *103*(C10), 21,531–21,542.
Pollard, R. T., and L. Regier (1990), Large variations in potential vorticity at small spatial scales in the upper ocean, *Nature*, *348*(6298), 227–229, doi:10.1038/348227a0.
Pollard, R. T., and L. A. Regier (1992), Vorticity and vertical circulation at an ocean front, *J. Phys. Oceanogr.*, *22*, 609–625.
Read, J. F., and R. T. Pollard (1992), Water masses in the region of the Iceland-Faeroes Front, *J. Phys. Oceanogr.*, *22*, 1365–1378.
Rossby, T., and C. N. Flagg (2012), Direct measurement of the volume flux in the Faroe-Shetland Channel and over the Iceland-Faroe Ridge, *Geophys. Res. Lett.*, *39*, L07602, doi:10.1029/2012GL051269.
Rossby, T., M. D. Prater, and H. Søiland (2009), Pathways of inflow and dispersion of warm waters in the Nordic seas, *J. Geophys. Res.*, *114*, C04011, doi:10.1029/2008JC005073.
Sarafanov, A., A. Falina, A. Sokov, and A. Demidov (2008), Intense warming and salinification of intermediate waters of southern origin in the eastern subpolar North Atlantic in the 1990s to mid-2000s, *J. Geophys. Res.*, *113*, C12022, doi:10.1029/2008JC004975.
Scott, J. C., and A. L. McDowall (1990), Cross-frontal cold jets near Iceland: In-water, satellite infrared, and geosat altimeter data, *J. Geophys. Res.*, *95*(C10), 18,005–18,014.
Smart, J. H. (1984), Spatial variability of major frontal systems in the North Atlantic-Norwegian Sea area: 1980-1981, *J. Phys. Oceanogr.*, *14*, 185–192.
Spall, M. A. (1995), Frontogenesis, subduction, and cross-front exchange at upper ocean fronts, *J. Geophys. Res.*, *100*(C2), 2543–2557, doi:10.1029/94JC02860.
Stendardo, I., and N. Gruber (2012), Oxygen trends over five decades in the North Atlantic, *J. Geophys. Res.*, *117*, C11004, doi:10.1029/2012JC007909.
Thomas, L. N., and T. M. Joyce (2010), Subduction on the Northern and Southern Flanks of the Gulf Stream, *J. Phys. Oceanogr.*, *40*(2), 429–438, doi:10.1175/2009jpo4187.1.
Thomas, L. N., and C. M. Lee (2005), Intensification of ocean fronts by down-front winds, *J. Phys. Oceanogr.*, *35*, 1086–1102.
Thomas, L. N., C. M. Lee, and Y. Yoshikawa (2010), The subpolar front of the Japan/East Sea. Part II: Inverse method for determining the frontal vertical circulation, *J. Phys. Oceanogr.*, *40*(1), 3–25, doi:10.1175/2009JPO4018.1.
Ullgren, J. E., I. Fer, E. Darelius, and N. L. Beaird (2014), Interaction of the Faroe Bank Channel overflow with Iceland Basin intermediate waters, *J. Geophys. Res. Oceans*, *119*, 228–240, doi:10.1002/2013JC009437.
van Aken, H. M., and C. J. de Boer (1995), On the synoptic hydrography of intermediate and deep water masses in the Iceland Basin, *Deep Sea Res., Part I*, *42*, 165–189.
Willebrand, J., and J. Meincke (1980), Statistical analysis of fluctuations in the Iceland-Scotland frontal zone, *Deep Sea Res., Part A*, *27*, 1047–1066.